Research Article | Open Access

Journal of Materials Informatics

Wu *et al. J. Mater. Inf.* **2026**, *6*, 42 **DOI:**10.20517/jmi.2026.31

Data-driven design of high-abundance rare earth permanent magnets for low-carbon and resource-efficient production

Yuxuan Wu[1,3], Qianqian Wang[2,*], Qihan Zhang[3], Shen Zhao[3], Qiangfeng Li[3], Dehai Wu[4], Fang Wu[4], Hongdong Yu[1,3], Lu Wang[1,3,4,*]

Keywords:
Machine learning, multi-objective optimization, rare earth permanent magnets, global warming potential, sustainable development

Citation: Wu, Y.; Wang, Q.; Zhang, Q.; Zhao, S.; Li, Q.; Wu, D.; Wu, F.; Yu, H.; Wang, L. Data-driven design of high-abundance rare earth permanent magnets for low-carbon and resource-efficient production. *J. Mater. Inf.* **2026**, *6*, 42. https://dx.doi.org/10.20517/jmi.2026.31

Received: 14 May 2026 **First Decision:** 18 Jun 2026 **Revised:** 17 Jul 2026 **Accepted:** 4 Aug 2026 **Published:** 27Aug 2026

Academic Editors: Xiaoyan Song, Xiaoyu Chong **Copy Editor:** Pei-Yun Wang **Production Editor:** Pei-Yun Wang

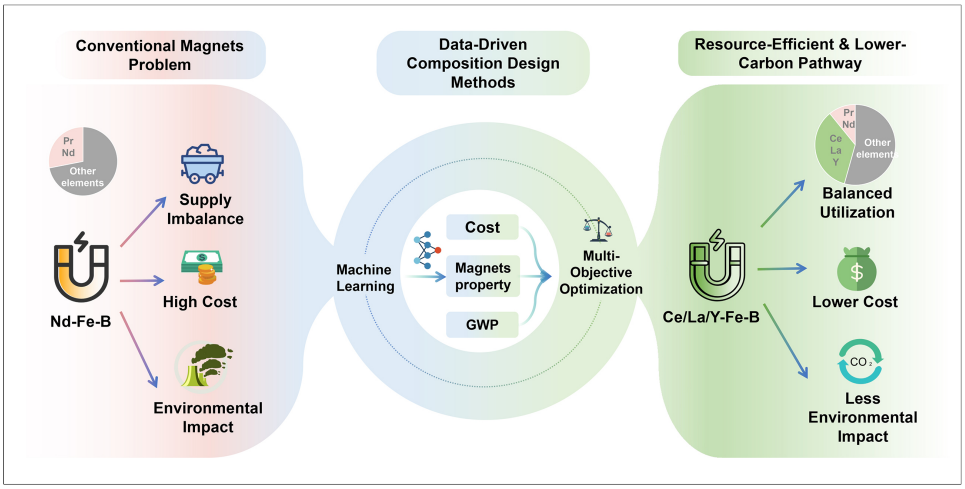

Abstract

Rare-earth permanent magnets are essential for renewable energy and electric vehicle technologies, but their dependence on critical rare-earth elements raises concerns regarding resource security, cost, and environmental impact. Here, we develop an integrated data-driven framework for the sustainable design of high-abundance rare-earth permanent magnets. A dataset containing 346 experimental samples was constructed to establish composition–property relationships for Br, H_{cj}, and $(BH)_{max}$. Eight machine learning (ML) algorithms were compared, and the multi-layer perceptron (MLP) model exhibited the most balanced overall performance after model refinement. The optimized MLP achieved testing R^2 values of 0.979, 0.901, and 0.955 for Br, H_{cj}, and $(BH)_{max}$, respectively, and repeated five-fold cross-validation supported its robustness. SHapley Additive exPlanations analysis indicated that Nd exerted the strongest statistical influence on the predicted magnetic properties, while Ce and La also contributed through nonlinear

[1]School of Rare Earths, University of Science and Technology of China, Hefei 230026, Anhui, China.
[2]School of Low-Altitude Technology and Engineering, Gannan College of Science and Technology, Ganzhou 341000, Jiangxi, China.
[3]Ganjiang Innovation Academy, Chinese Academy of Sciences, Ganzhou 341119, Jiangxi, China.
[4]Key Laboratory of Ionic Rare Earth Resources and Environment, Ministry of Natural Resources of the People's Republic of China, Ganzhou 341000, Jiangxi, China.

***Correspondence to:** Prof. Qianqian Wang, School of Low-Altitude Technology and Engineering, Gannan College of Science and Technology, Ganzhou 341000, Jiangxi, China. E-mail: wangqianqian_cn@163.com; Prof. Lu Wang, Ganjiang Innovation Academy, Chinese Academy of Sciences, Ganzhou 341119, Jiangxi, China. E-mail: lwang@gia.cas.cn

composition-property associations. The optimized MLP model was subsequently integrated with non-dominated sorting genetic algorithm II and Technique for Order Preference by Similarity to Ideal Solution to balance predicted $(BH)_{max}$, material cost, and a composition-related upstream global warming potential (GWP) indicator. The selected Ce-rich candidate achieved a predicted $(BH)_{max}$ of 35.16 MGOe, an estimated material cost of 4.78 $/kg, and a GWP indicator of 16.41 kg CO_2-eq/kg. These results demonstrate the potential of interpretable ML combined with multi-objective optimization for screening resource-efficient permanent-magnet compositions.

INTRODUCTION

Rare earth elements (REEs) play an essential role in modern technologies, particularly in renewable energy systems, electric vehicles, and advanced electronic devices[1]. Among rare earth-based functional materials, Nd-Fe-B permanent magnets exhibit among the highest commercial magnetic performance and are indispensable components in many low-carbon technologies[2]. However, the extensive dependence on critical REEs, especially Nd, Pr, Dy, and Tb, has raised significant concerns regarding resource availability, supply chain vulnerability, and environmental impacts associated with rare earth extraction and processing[3]. Therefore, developing permanent magnets with reduced dependence on critical elements while maintaining competitive magnetic performance has become an important research priority.

From the perspective of resource sustainability, high-abundance REEs, including Ce, La, and Y, represent attractive substitutes because of their relatively large reserves and lower supply risks[4]. However, their application in high-performance permanent magnets remains challenging due to their distinct electronic structures and weaker intrinsic magnetic properties compared with Nd-based systems[5]. In addition, complex phase equilibria, compositional interactions, and processing-dependent microstructural evolution further restrict the optimization of high-abundance rare earth permanent magnets. Significant progress has nevertheless been achieved through compositional engineering and microstructural regulation. Zhu *et al.* developed (Ce, Nd)-Fe-B dual-phase magnets, achieving a high maximum magnetic energy product while reducing Nd consumption through optimized phase formation[6]. Industrial production of (Ce, Nd)-Fe-B sintered magnets further demonstrated the feasibility of utilizing high-abundance REEs in commercial permanent magnets[7]. Elemental doping strategies have also been widely investigated, among which Co addition has been reported to effectively improve Curie temperature while maintaining acceptable magnetic properties[8]. Recent work further showed that grain boundary diffusion strategies can significantly enhance the coercivity of high-Ce Nd-Ce-Fe-B magnets by optimizing phase evolution and Dy diffusion behavior, offering an effective route for improving the performance of Ce-rich permanent magnets[9]. Despite these advances, optimizing multi-component rare earth permanent magnets through conventional experimental approaches remains inefficient because of the enormous compositional space and complicated nonlinear relationships between composition and magnetic properties.

Recent advances in artificial intelligence and machine learning (ML) have provided new opportunities for accelerating materials design[10,11]. By learning complex nonlinear relationships between composition and properties from experimental data, ML models can significantly improve prediction accuracy and reduce experimental costs[12]. Several studies have demonstrated the feasibility of ML-assisted design for rare earth permanent magnets. Cheng developed a hybrid prediction-optimization framework combining support vector regression (SVR) with particle swarm optimization (PSO) to model the relationship between NdFeB composition and remanence, achieving a coefficient of determination (R^2) of 0.839[13]. Zhang *et al.* employed multiple linear regression to derive an empirical remanence model for Zr/Co-alloyed $Nd_2Fe_{14}B$ magnets and further improved prediction accuracy by constructing physically meaningful feature descriptors[14]. More recently, Qiao *et al.* established ML models to predict the remanence and coercivity of sintered NdFeB magnets based on compositional and processing parameters, achieving high prediction accuracy[15].

Collectively, these studies highlight the strong potential of ML-based methodologies for guiding the efficient design and optimization of rare earth permanent magnets.

However, these existing ML-assisted studies still have several limitations. First, most previous studies mainly focus on predicting individual magnetic properties, while selecting optimal compositions under multiple practical constraints remains underexplored. Second, economic factors, resource availability, and environmental impacts are rarely considered simultaneously during material optimization. In sustainable materials design, achieving high performance alone is insufficient; material cost, resource efficiency, and environmental burden should also be incorporated into the design framework. Third, although ML models provide powerful prediction capability, their limited interpretability restricts the understanding of composition–property relationships and reduces their ability to provide mechanistic guidance for experimental design.

Multi-objective optimization provides an effective strategy for solving complex engineering problems involving competing objectives by identifying Pareto-optimal solutions[16]. Its core objective is to identify one or more Pareto-optimal solutions that balance competing goals, and it has been widely applied in engineering design[17], resource allocation[18], environmental management[19], financial investment[20], and material design [21]. Zhang *et al.* conducted a multi-objective evaluation and process optimization of the V_2O production process from the perspectives of life cycle assessment, integrated environmental evaluation, and economic evaluation[22]. Zeraati *et al.* synthesized Fe–Co–Ni nanostructured ternary alloys using mechanical and evolutionary approaches and optimized their magnetic properties through multi-objective artificial neural networks (ANNs) combined with genetic algorithms (GAs)[23]. Wakjira *et al.* accurately predicted the strength of ultra-high-performance concrete (UHPC) using ML models, incorporating strength, cost, and 17 environmental impact categories as objective functions for multi-objective optimization, providing a comprehensive assessment of the environmental sustainability of UHPC mixes[24]. These studies demonstrate that multi-objective optimization can effectively coordinate material performance, resource consumption, and environmental impact, thereby providing strong support for sustainable material design.

Motivated by these advances, this study develops an integrated data-driven framework for the sustainable design of high-abundance rare earth permanent magnets, as shown in Figure 1. A comprehensive dataset comprising 346 experimental samples was constructed to model key magnetic properties, including remanence (Br), coercivity (H_{cj}), and maximum energy product [$(BH)_{max}$]. Multiple ML algorithms were evaluated, and the optimal model was further interpreted using SHapley Additive exPlanations (SHAP) to reveal the underlying compositional effects. Building upon the predictive model, a multi-objective optimization framework integrating the non-dominated sorting genetic algorithm II (NSGA-II) and the Technique for Order Preference by Similarity to Ideal Solution (TOPSIS) was developed to simultaneously optimize magnetic performance, economic cost, and global warming potential (GWP). This framework provides a systematic approach for integrating ML, life cycle assessment, and multi-objective optimization in advanced materials design.

MATERIALS AND METHODS

Datasets development and preprocessing

Datasets development

In this study, a comprehensive database was constructed based on published literature on high-abundance rare-earth permanent magnets. The database contains detailed information on chemical composition and key magnetic properties, including Br, H_{cj}, and $(BH)_{max}$. The data were collected from articles published between 1997 and 2024, retrieved from the Web of Science, Google Scholar, and CNKI databases. The nominal composition was represented by ten input variables: P_{Ce}, P_{La}, P_Y, P_{Pr}, P_{Nd}, P_{REs}, P_{Fe}, P_{Co}, P_{TM} and P_B.

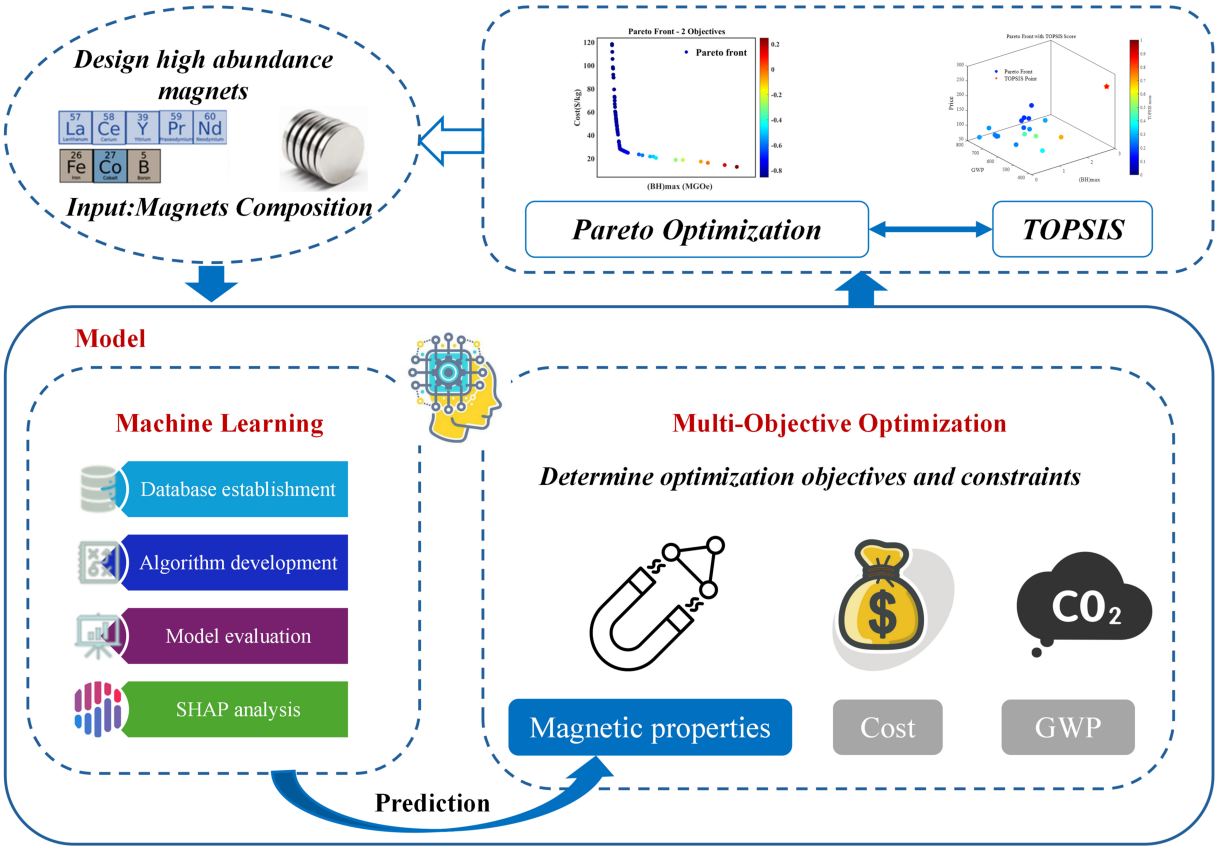

Figure 1. Framework for multi-objective optimization of high-abundance magnets based on ML. ML: Machine learning; TOPSIS: Technique for Order Preference by Similarity to Ideal Solution; SHAP: SHapley Additive exPlanations analysis; GWP: global warming potential.

Here, the first five variables represent the normalized fractions of the individual rare-earth elements within the total rare-earth content, whereas the remaining five variables represent their mass percentages or component contents in the whole magnet. The whole magnets can be expressed as $(Ce_{P_{Ce}} La_{P_{La}} Y_{P_Y} Pr_{P_{Pr}} Nd_{P_{Nd}})_{P_{REs}} Fe_{P_{Fe}} Co_{P_{Co}} TM_{P_{TM}} B_{P_B}$. ML models were subsequently employed to establish the nonlinear relationships between composition and magnetic properties, enabling composition-property prediction of high-abundance rare-earth permanent magnets.

The final dataset contained 346 records. Although this sample size is larger than that of many individual experimental studies, it remains limited for complex ML models. Accordingly, the dataset was used primarily to establish a preliminary composition-property surrogate model within the compositional domain covered by the collected literature. Predictions outside the observed data range were not regarded as experimentally validated results.

Based on the established ML database for magnetic property prediction, a multi-objective optimization database was further developed by incorporating economic cost and environmental impact indicators. Specifically, the GWP and economic cost associated with each constituent element were collected from published literature. GWP data were obtained from published life-cycle inventories covering upstream production of the constituent elements, primarily from raw-material extraction to the metal-production stage. For elements with multiple reported values, qualified data points were averaged to ensure data reliability and consistency. Economic cost data were derived from market prices. The prices of rare-earth metals with purities above 99% were obtained from reported average market prices. The cost of iron was

approximated using the price of pure iron, while the cost of boron was estimated based on the market price of ferroboron. These datasets collectively enable a quantitative evaluation of trade-offs among magnetic performance, economic cost, and carbon emissions in the subsequent multi-objective optimization analysis.

Data screening and preprocessing

Duplicate records were identified using the combination of nominal composition, processing condition, and reported magnetic properties. Exact duplicates were removed, whereas records with identical nominal compositions but different processing routes were retained as independent observations when the original source reported distinct experimental results.

Records missing any of the three target properties were excluded from the corresponding target-specific model but could be retained for the other targets when the required input variables were available. Missing composition values were interpreted as zero only when the original article explicitly indicated that the element was absent; otherwise, the record was treated as incomplete and excluded. No target value was imputed.

Potential outliers were first screened using physical and reporting criteria, including impossible negative compositions, mass fractions inconsistent with the nominal formula, and property values outside physically meaningful ranges. Statistical outliers were then identified using the interquartile-range criterion within each target variable. However, a statistically extreme value was removed only when it could be traced to a transcription, unit-conversion, or reporting error. Valid extreme experimental observations were retained to avoid artificially narrowing the data distribution.

After screening, 11 records were removed as duplicates, 24 records were excluded because of missing information, and 15 records were corrected or removed because of unit or transcription errors. The final dataset contained 346 samples.

ML model

Algorithm development

To avoid selecting a regression model a priori, eight representative algorithms with different learning mechanisms were systematically benchmarked, including gradient boosting decision trees (GBDT), kernel extreme learning machine (KELM), k-nearest neighbors (KNN), light gradient boosting machine (LightGBM), SVR, least squares support vector machine (LSSVM), random forest (RF), and multi-layer perceptron (MLP). These algorithms represent tree-based ensemble methods, kernel-based methods, instance-based learning, and neural-network-based nonlinear regression[25].

Because the three target properties, Br, H_{cj}, and $(BH)_{max}$, have different numerical ranges and composition sensitivities, an independent model was trained for each algorithm–property combination. Therefore, 24 regression models were evaluated in total. The purpose of this comparison was not to increase the number of models unnecessarily, but to determine whether the same learning algorithm could provide consistently reliable predictions across all three magnetic properties under a unified data-splitting and evaluation protocol. All algorithms were trained and evaluated using the same input features, training/test partitions, preprocessing procedures, and performance metrics to ensure a fair comparison.

To determine an appropriate training and test partition strategy, three splitting ratios (70%:30%, 80%:20%, and 90%:10%) were compared. Model performance was evaluated using independent test R^2 values and repeated five-fold cross-validation results. Although the optimal split varied among different magnetic

properties, the 80%:20% partition provided the best overall balance between training data availability and generalization evaluation. Therefore, this ratio was adopted for subsequent model development.

All model development was conducted in the PyCharm environment, with data processing and ML methods using the open-source scikit-learn library, and the programming language was Python (version 3.11). The detailed parameters of the MLP model are provided in the Supplementary Table 1. To enhance the robustness and credibility of the models, five-fold cross-validation was repeated. The model prediction performance was evaluated using R^2[26], root mean squared error (RMSE)[27], and mean absolute error (MAE)[27], with the calculation method in Equations (1)-(3).

$$R^2 = 1 - \frac{\sum_{i=1}^{N}\left(y_p^i - y_t^i\right)^2}{\sum_{i=1}^{N}\left(y_t^i - y_m\right)^2} \tag{1}$$

$$RMSE = \sqrt{\frac{\sum_{i=1}^{N}\left(y_t^i - y_p^i\right)^2}{N}} \tag{2}$$

$$MAE = \frac{\sum_{i=1}^{N}\left|y_t^i - y_p^i\right|}{N} \tag{3}$$

where y_p^i is the predicted value, y_t^i is the true value collected from the previous articles, y_m is the mean value, and N is the number of data points in the training, testing, or verification datasets.

Feature importance analysis

Since most ML models are regarded as black-box approaches, the underlying relationships between input features and predicted magnetic properties are often difficult to interpret. To address this limitation, the SHAP method was used for feature visualization and interpretability analysis[28]. The SHAP framework quantifies the contribution of each input feature to individual predictions by calculating Shapley values based on cooperative game theory. These values indicate both the magnitude and direction (positive or negative) of feature effects on the predicted outcomes. Compared with conventional feature importance methods that only provide global rankings, SHAP enables a more comprehensive interpretation of feature contributions at both global and individual sample levels, thereby providing deeper insights into the composition-property relationships of high-abundance rare earth permanent magnets.

Multi-objective optimization

Objective functions

This multi-objective optimization model consists of three objective functions: the MLP-based magnetic performance prediction model, the GWP linear function, and the economic cost linear function. The magnetic performance prediction function uses the MLP model to predict $(BH)_{max}$ as the objective function f_1. The GWP and economic cost are calculated using composition-weighted linear functions, with the specific calculation methods as shown in Equations (4) and (5).

$$f_2\left(GWP, kg\ CO_2 - eq/kg\right) = \frac{1}{100}\{P_{REs}(P_{Ce} \times GWP_{Ce} + P_{La} \times GWP_{La} + P_Y \times GWP_Y + P_{Pr} \times GWP_{Pr} + P_{Nd} \times GWP_{Nd}) + P_{Fe}GWP_{Fe} + P_BGWP_B + P_{Co}GWP_{Co}\} \tag{4}$$

$$f_3(Cost, \$/kg) = \frac{1}{100}\{P_{REs}(P_{Ce} \times C_{Ce} + P_{La} \times C_{La} + P_Y \times C_Y + P_{Pr} \times C_{Pr} + P_{Nd} \times C_{Nd}) + P_{Fe} \times C_{Fe} + P_B \times C_B + P_{Co} \times C_{Co}\} \tag{5}$$

Where the variables P_{Ce}, P_{La}, P_Y, P_{Pr}, P_{Nd}, P_{Fe}, P_B, P_{Co}, P_{REs} represent the contents of Ce, La, Y, Pr, Nd, Fe, B, Co and total REEs, respectively. The values GWP_{Ce}, GWP_{La}, GWP_Y, GWP_{Pr}, GWP_{Nd}, GWP_{Fe}, GWP_B, GWP_{Co} represent the GWP values corresponding to Ce, La, Y, Pr, Nd, Fe, B, and Co. The variables C_{Ce}, C_{La}, C_Y, C_{Pr},

Table 1. Unit GWP and price of components of high-abundance magnets

Components	GWP (kg CO_2-eq/kg)	Unit price ($/kg)
Ce	10.41[29,30]	3.53
La	13.21[29]	0.57
Y	12.61[30]	33.21
Pr	79.31[29]	62.03
Nd	95.01[31]	76.15
Fe	13.32[32]	0.72
Co	11.73[33]	23.31
B	0.49[34]	3.35

GWP: Global warming potential.

C_{Nd}, C_{Fe}, C_B, C_{Co} correspond to the economic costs (unit price) of Ce, La, Y, Pr, Nd, Fe, B, and Co, respectively. The GWP values for each element were obtained from the literature, as shown in Table 1. Since TM corresponds to various metals and only a small amount of magnet data includes this, its impact on the results is minimal, and therefore the GWP and economic costs for other metals are not considered. The cost values were estimated by the average price of each metal (purity ≥ 99%) in 2024 published on CBC Metals (https://www.cbcie.com/).

The environmental objective in this study is a composition-based upstream GWP proxy rather than a full cradle-to-grave LCA of a finished magnet. The included processes correspond primarily to the production of the constituent elements up to the metal stage, according to the system boundaries of the source inventories. Magnet manufacturing stages, including alloy melting, strip casting, hydrogen decrepitation, jet milling, magnetic alignment, pressing, sintering, heat treatment, machining, coating, transportation, use, collection, and recycling, were not modeled.

The total objective function F consists of these three objective functions, with the goal of maximizing f_1 and minimizing f_2 and f_3.

$$F = \begin{cases} max f_1(maximum\ magnetic\ energy\ product) \\ min f_2(GWP) \\ min f_3(Cost) \end{cases} \tag{6}$$

Constraints

The primary constraints of the objective function are defined by the structural requirements of the magnet and include both equality and inequality constraints. These constraints ensure that the designed magnetic material satisfies the desired chemical composition and physical properties, in accordance with established principles of materials design. Firstly, to characterize the nominal composition of the magnet, the sum of the proportions of the REEs (Ce, La, Y, Pr, and Nd) is constrained to equal 1, as shown in Equation (7). This constraint ensures that the relative fractions of Ce, La, Y, Pr, and Nd within the total rare-earth sublattice sum to unity, which is consistent with standard design practices for multi-component alloys and ensures compositional integrity as well as magnetic and chemical stability. Second, the sum of the mass percentages of REs, Fe, B, TM, and Co is set to 100, as shown in Equation (8). This constraint reflects the material balance requirement in alloy or composite material design. Finally, since the subject of this study is rare earth iron-boron permanent magnets, it is essential that the material contains REEs, iron, and boron. To prevent the complete omission of certain essential elements during the synthesis process, we specify that the proportions

of REs, Fe, and B must be greater than zero, as shown in Equation (9). Collectively, these constraints ensure compositional feasibility and provide a sound theoretical basis for subsequent optimization of magnetic performance.

$$P_{Ce} + P_{La} + P_Y + P_{Pr} + P_{Nd} = 1 \tag{7}$$

$$P_{REs} + P_{Fe} + P_B + P_{Co} + P_{TM} = 100 \tag{8}$$

$$P_{REs}, P_{Fe}, P_B, P_{Co} > 0 \tag{9}$$

NSGA-II algorithm and TOPSIS method

We use the NSGA-II algorithm to solve the multi-objective optimization problem. This algorithm, developed by Deb *et al.*[35], based on the Pareto method, has been proven to be an effective algorithm for solving multi-objective optimization problems[36]. The algorithm divides the population hierarchy through non-dominated sorting and maintains solution diversity using crowding distance, enabling rapid convergence to the Pareto front. To identify a final optimal solution from the Pareto-optimal set, TOPSIS, a multi-criteria decision-making method, is required[37]. This method selects the solution that is furthest from the negative ideal point (the worst solution) and closest to the positive ideal point (the best solution). The positive (d_{i+}) and negative (d_{i-}) ideal points are given by Equations (10) and (11). The closeness coefficient is calculated according to Equation (12), and the final optimal solution is the one with the highest C_i value[38].

The overall algorithmic workflow of this study is summarized as follows. First, an initial population of 700 individuals is generated using a customized initialization function. Each individual consists of 10 decision variables that satisfy the imposed constraints, where the sum of the first five rare earth variables equals 1, and the sum of the last five variables equals 100. The objective functions calculate the three target values using the pre-trained MLP model and two sets of linear functions. Individuals that violated the imposed constraints were assigned penalty values. During optimization, NSGA-II maintains population diversity through non-dominated sorting and crowding distance. Tournament selection is employed with a crossover probability of 0.7 and a mutation probability of 0.3. After 500 iterations, the parent and child populations are merged, and the Pareto front is extracted. Finally, the TOPSIS method is applied to evaluate the comprehensive performance of the Pareto-optimal solutions and identify the final optimal design. This integrated optimization framework enables efficient and reliable resolution of complex engineering optimization problems. The upper and lower bounds of each decision variable, along with other algorithm parameters, are shown in the Supplementary Table 2.

$$d_{i+} = \sqrt{\sum_{j=1}^{n} \left(F_{ij} - F_j^{ideal}\right)^2} \tag{10}$$

$$d_{i-} = \sqrt{\sum_{j=1}^{n} \left(F_{ij} - F_j^{non-ideal}\right)^2} \tag{11}$$

$$C_i = \frac{d_{i-}}{d_{i+} + d_{i-}} \tag{12}$$

where i represents a Pareto solution, n is the number of objectives, F_j^{ideal} and $F_j^{non\text{-}ideal}$ represent the ideal and non-ideal objective values for the j-th single-objective optimization problem, and C_i is the closure coefficient.

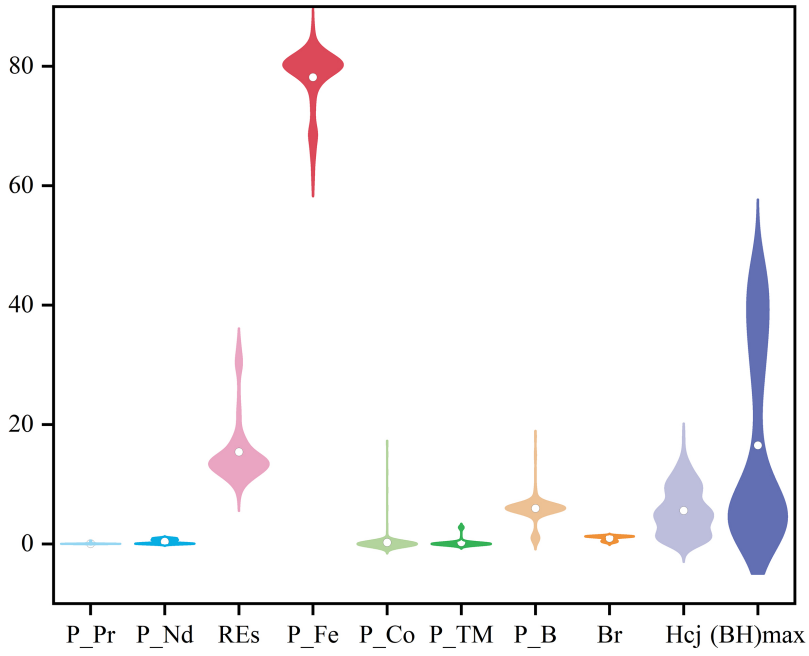

Figure 2. Violin map of all input and output features.

RESULTS AND DISCUSSION

Data distribution and correlation analysis

To systematically evaluate the characteristics of the datasets and their potential influence on magnetic performance prediction, statistical analysis and visualization were first conducted to examine the distribution patterns and correlations between input variables and output targets, as shown in Figures 2 and 3 and Supplementary Table 3. This analysis provides an overview of the data structure, offers guidance for subsequent data preprocessing and feature engineering, and preliminarily reveals interaction trends among the variables.

Range-based statistical analysis plays a crucial role in identifying potential outliers and assessing data variability, thereby supporting robust model development. Supplementary Table 3 summarizes the minimum, maximum, and other relevant statistics for each feature, enabling a quantitative evaluation of their distributions. As shown in Figure 2, the value ranges of different features vary considerably: some variables exhibit wide distributions, while others are relatively concentrated. As a result, we applied data normalization to mitigate the potential adverse effects of scale differences on model stability and prediction accuracy.

To further investigate feature correlations, Figure 3 presents the Pearson correlation heatmap of the datasets. The Pearson correlation coefficient provides a quantitative measure of linear dependence between variables and serves as a preliminary tool for feature selection and model construction. Values approaching 1 or -1 indicate strong positive or negative linear relationships, respectively, whereas values between -0.5 and 0.5 suggest weak linear correlations. The correlation analysis provides preliminary insights into the statistical relationships between composition variables and magnetic properties. Nd shows a strong positive correlation with Br and $(BH)_{max}$, confirming its critical contribution to high magnetic performance. In contrast, high-abundance REEs, including Ce, La, and Y, exhibit relatively weaker or negative correlations, reflecting the intrinsic challenge of replacing Nd while maintaining magnetic properties.

However, Pearson correlation only captures linear relationships and cannot fully describe the complex nonlinear interactions among multiple alloying elements. Therefore, all composition variables were retained

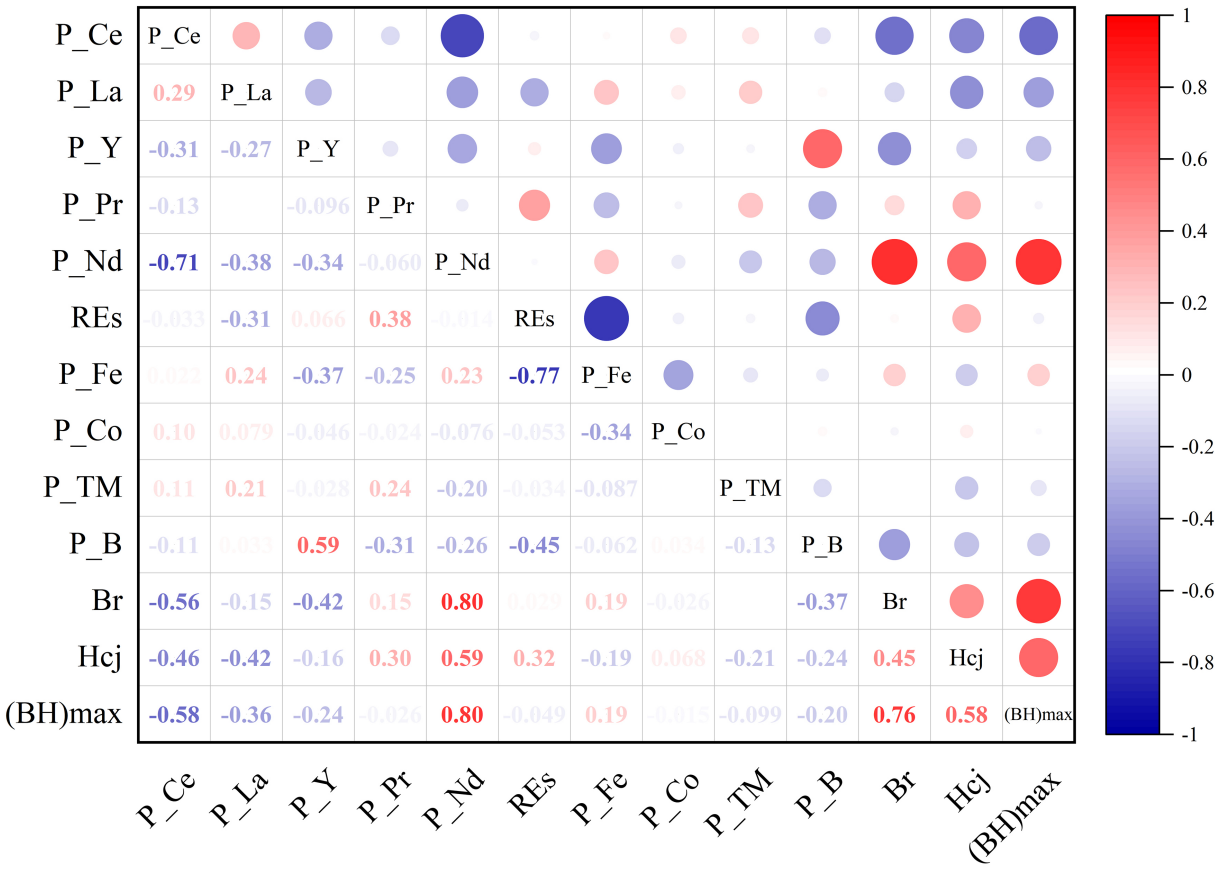

Figure 3. Correlation heatmap of all input and output variables.

as input features for subsequent ML modeling, where nonlinear algorithms were employed to identify hidden composition–property relationships.

Model development and performance comparisons

To identify an appropriate prediction algorithm without prior assumptions, eight representative ML algorithms with different learning mechanisms were initially evaluated, including ensemble learning methods (GBDT, LightGBM, and RF), kernel-based methods (SVR, KELM, and LSSVM), instance-based learning (KNN), and neural-network-based regression (MLP). These models were trained using identical input features, data preprocessing procedures, and evaluation criteria to ensure a fair comparison.

The preliminary comparison results are summarized in Table 2 and Supplementary Figures 1-3, indicating that the nonlinear relationship between elemental composition and magnetic properties cannot be equally captured by different algorithms. For Br prediction, LSSVM achieved the highest R^2 value (0.89), while MLP obtained an R^2 value of 0.77 and showed comparable performance with several other nonlinear models. For H_{cj} prediction, LSSVM slightly outperformed MLP, with R^2 values of 0.91 and 0.89, respectively. For $(BH)_{max}$ prediction, MLP achieved the highest R^2 value of 0.91, demonstrating superior prediction capability compared with the other evaluated algorithms. Considering the overall prediction performance across the three magnetic properties, including accuracy, consistency, and balance among different targets, the MLP model was selected as the surrogate model for subsequent optimization.

To further improve the prediction capability of the MLP, hyperparameter optimization was subsequently performed. Considering that the dataset contains a relatively limited number of experimental samples, the

Table 2. Performance parameters of the applied models

Prediction model	Br			H_{cj}			$(BH)_{max}$		
	RMSE	MAE	R^2	RMSE	MAE	R^2	RMSE	MAE	R^2
GBDT	0.06	0.05	-2.23	2.84	2.17	-1.39	5.98	5.25	-3.30
LightGBM	0.06	0.05	-2.42	3.09	2.52	-1.83	6.52	6.00	-4.10
RF	0.10	0.09	-7.48	3.77	3.30	-3.22	12.01	11.66	-16.32
SVR	0.12	0.12	-11.26	2.33	2.09	-0.61	5.25	5.19	-2.31
KNN	0.09	0.08	-6.44	4.10	3.55	-3.98	6.76	6.46	-10.44
KELM	0.08	0.07	-4.16	3.03	2.61	-1.71	6.22	6.05	-8.68
LSSVM	0.01	0.01	0.89	0.56	0.35	0.91	1.55	1.13	0.71
MLP	0.02	0.01	0.77	0.60	0.39	0.89	0.46	0.34	0.91

RMSE: Root mean squared error; MAE: mean absolute error; R^2: coefficient of determination; GBDT: gradient boosting decision trees; LightGBM: light gradient boosting machine; RF: random forest; SVR: support vector regression; KNN: k-nearest neighbors; KELM: kernel extreme learning machine; LSSVM: least squares support vector machine; MLP: multi-layer perceptron.

model complexity was carefully controlled during optimization. Bayesian optimization was applied to determine suitable training parameters, including learning rate, L2 regularization coefficient, and batch size. Meanwhile, the original network structure was adjusted to a more compact architecture consisting of three hidden layers with 128, 64, and 32 neurons, respectively. This optimized structure reduced unnecessary model parameters while maintaining sufficient nonlinear fitting ability.

The influence of different dataset partitioning strategies on model performance was further investigated. As shown in Figure 4, three train/test splitting ratios (70:30, 80:20, and 90:10) were compared for predicting Br, H_{cj}, and $(BH)_{max}$. The results reveal that model performance was sensitive to the data partition strategy. The 70:30 split resulted in relatively lower prediction performance, which can be attributed to the reduced number of samples available for model training. Although the 90:10 split provided more training samples, the smaller testing dataset increased the uncertainty of model evaluation. Among the three strategies, the 80:20 split exhibited the best overall balance between training efficiency and evaluation reliability, and was therefore selected for subsequent model construction.

Using the optimized architecture and selected data partition strategy, the final MLP model demonstrated improved prediction performance for all three magnetic properties. The comparison between experimental and predicted values is presented in Figure 5. The predicted results show strong agreement with experimental measurements, with testing R^2 values of 0.979, 0.901, and 0.955 for Br, H_{cj}, and $(BH)_{max}$, respectively. The relatively small deviation between predicted and experimental values indicates that the optimized MLP model successfully captures the composition–property relationships within the investigated compositional space. The residual distributions of the optimized MLP model are further analyzed in Supplementary Figure 4. The relatively concentrated residuals and the absence of obvious systematic deviations suggest that the model predictions are generally consistent with the experimental observations.

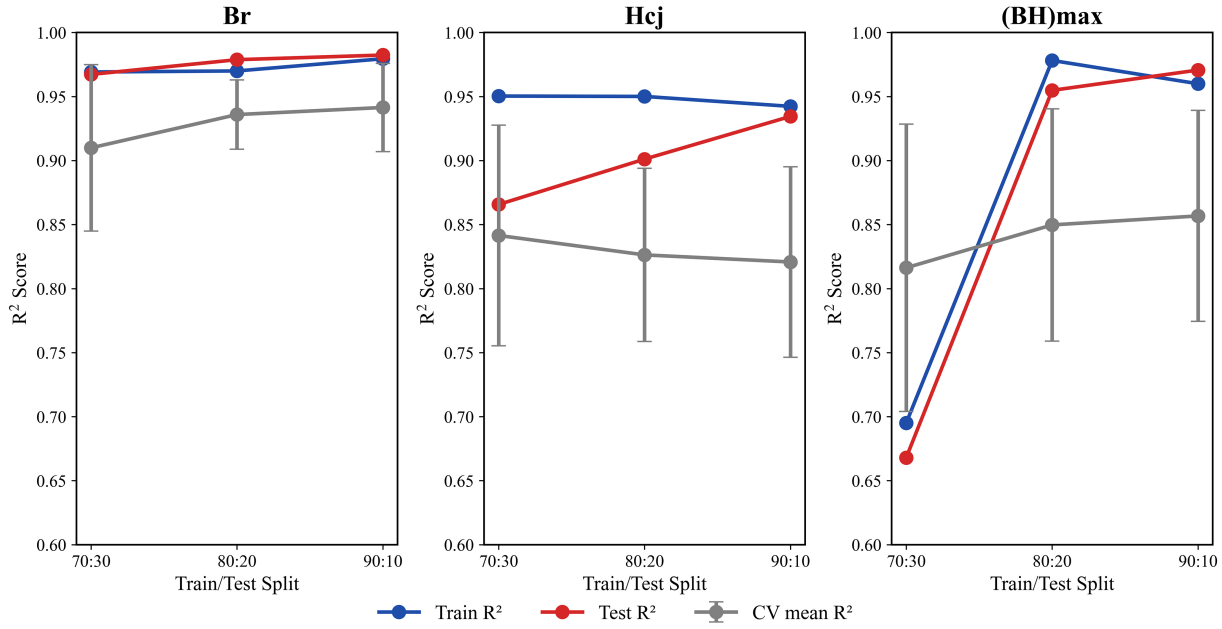

Figure 4. Sensitivity analysis of different train/test splitting ratios on MLP prediction performance for Br, H_{cj}, and $(BH)_{max}$. MLP: Multi-layer perceptron; R^2: coefficient of determination; CV: cross-validation.

To further evaluate the robustness of the optimized model, repeated five-fold cross-validation was performed. The average cross-validation R^2 values were 0.936 ± 0.027, 0.826 ± 0.068, and 0.850 ± 0.091 for Br, H_{cj}, and $(BH)_{max}$, respectively [Supplementary Table 4]. Although the cross-validation performance was slightly lower than that obtained from the independent test set, the prediction capability remained stable across different data subsets. This consistency demonstrates that the model performance was not solely dependent on a specific data split, but originated from the learned nonlinear relationship between composition and magnetic properties.

Overall, the optimized MLP model provides an accurate and robust surrogate model for subsequent multi-objective optimization[39]. However, because the dataset was collected from literature-reported experiments with different processing conditions, the model predictions should be regarded as data-driven screening results, and the optimized compositions require further experimental verification.

Feature importance analyses (SHAP)

Although the optimized MLP model exhibited excellent predictive performance, the nonlinear nature of neural-network-based models makes it difficult to directly understand the contribution of individual elemental components to magnetic properties. Therefore, SHAP analysis was performed to interpret the prediction behavior of the optimized MLP model and identify the dominant compositional factors associated with magnetic performance.

Figure 6A presents the global feature importance obtained from SHAP analysis. Among all input variables, Nd content is the most influential variable within the learned composition–property relationship. This result is consistent with the established understanding that Nd-based compounds possess strong magnetocrystalline anisotropy and consistent with the known importance of Nd-containing phases in high-performance permanent magnets. In addition to Nd, La, Ce, and other rare-earth elements also show considerable contributions, suggesting that the model captures complex composition-dependent interactions among different rare-earth components rather than relying on a single dominant element.

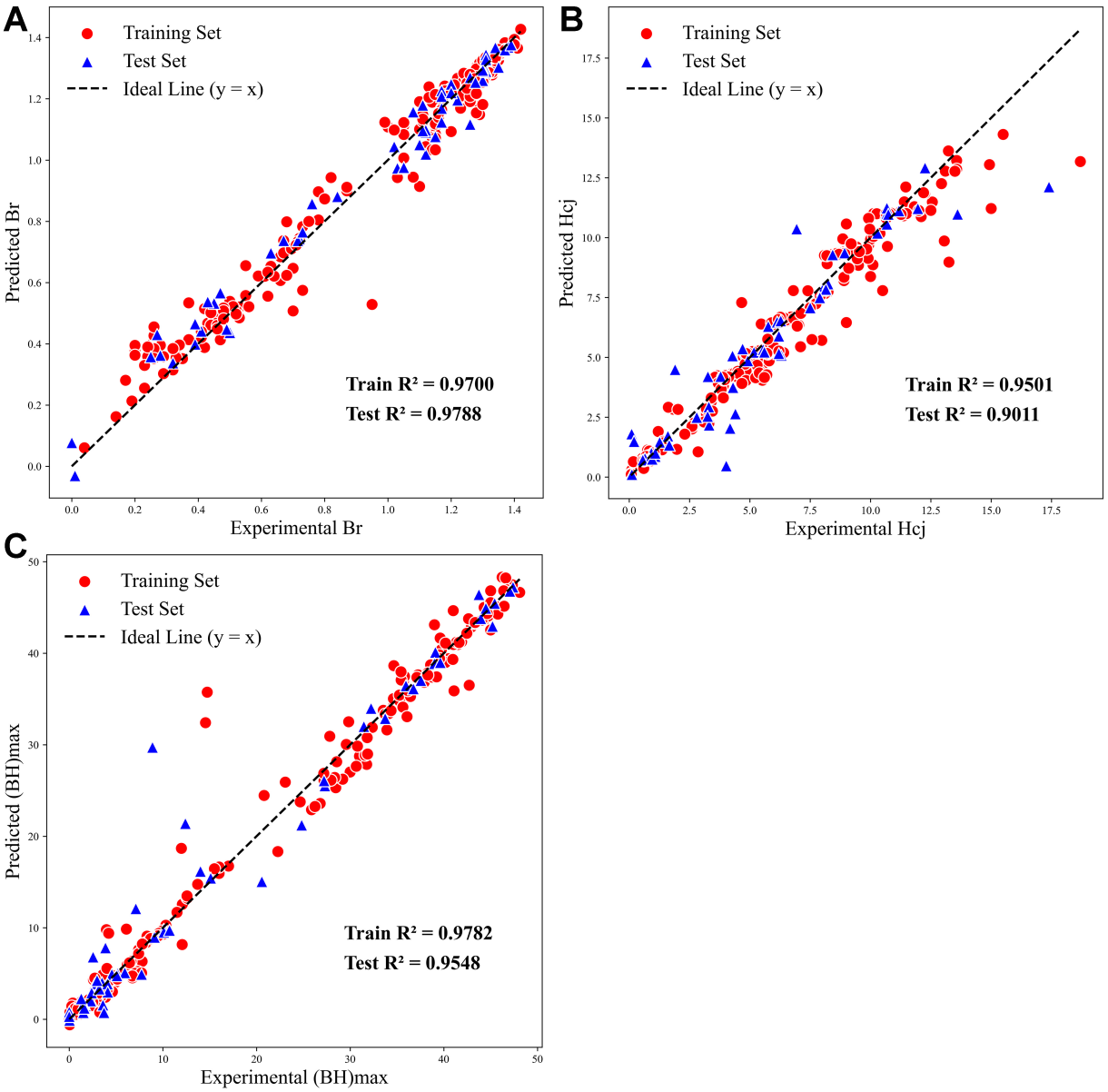

Figure 5. Prediction results of the MLP model for three output features with R^2 values for training and test sets. (A) Br; (B) H_{cj}; (C) $(BH)_{max}$. MLP: Multi-layer perceptron; R^2: coefficient of determination.

The SHAP contribution distribution further reveals that the influence of elemental composition is highly nonlinear. As shown in Figure 6B, the same element may have different effects depending on its concentration range and interactions with other alloying elements. For example, increasing Nd content generally corresponds to positive SHAP contributions to predicted magnetic performance across the analyzed composition range, whereas the contribution of high-abundance elements such as Ce and La depends strongly on their concentration levels and interactions with other components. This indicates that the relationship between composition and magnetic properties cannot be fully described by simple linear correlations, highlighting the advantage of ML approaches for exploring complex multicomponent magnet systems.

Among the high-abundance rare-earth elements, La shows a relatively significant contribution in the SHAP analysis. This statistical importance suggests that La-containing compositions may occupy an important region in the composition-property space learned by the model. Previous studies have reported that La

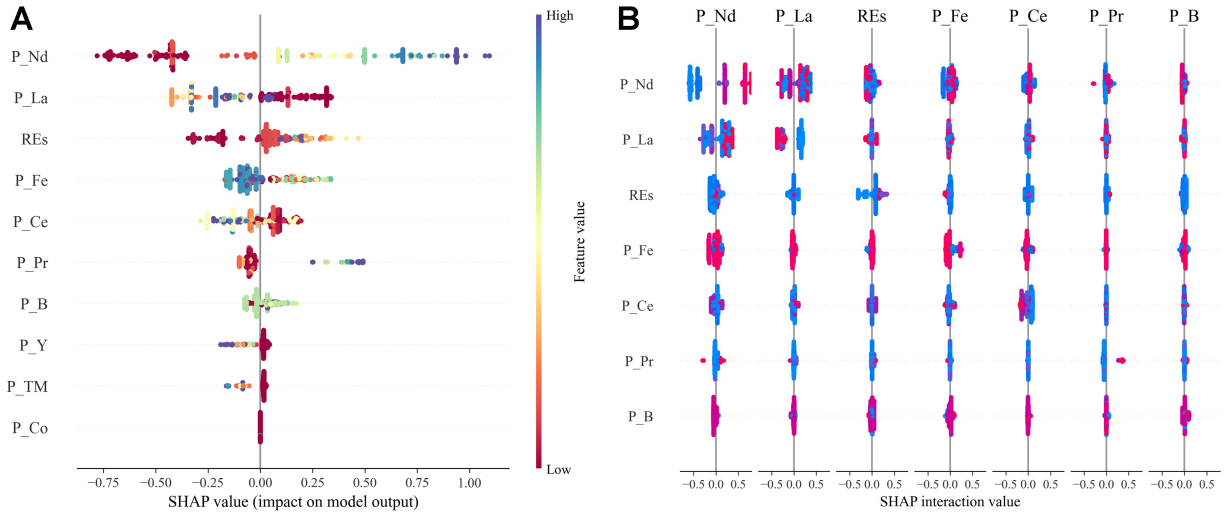

Figure 6. SHAP-based interpretation of the optimized MLP model. (A) Feature importance ranking showing the contribution of elemental composition variables to magnetic property prediction. (B) SHAP dependence plots illustrating nonlinear relationships and interaction effects between composition variables and model outputs. SHAP: SHapley Additive exPlanations analysis; MLP: multi-layer perceptron.

addition can influence phase formation, grain-boundary characteristics, and magnetic behavior in rare-earth iron-boron systems[40,41]. However, it should be emphasized that SHAP values represent statistical contributions to model predictions rather than direct evidence of specific physical mechanisms. Since processing parameters, phase fractions, and microstructural descriptors were not included as model inputs in the present study, the underlying physical origins of the identified associations require further experimental investigation.

Overall, SHAP analysis provides an interpretable connection between the machine-learning prediction model and the compositional design strategy. By identifying the relative importance and interaction effects of elemental variables, the analysis offers guidance for selecting promising composition regions and supports the subsequent multi-objective optimization process.

Multi-objective optimization

Based on the optimized MLP surrogate model, a multi-objective optimization framework was established to explore the compositional design space of high-abundance rare-earth permanent magnets. Unlike conventional optimization strategies that mainly focus on maximizing magnetic performance, the present framework simultaneously considers three competing objectives: maximizing predicted magnetic performance [$(BH)_{max}$], minimizing economic cost, and reducing composition-related environmental impact (GWP). The NSGA-II algorithm was employed to search for Pareto-optimal compositions, and the TOPSIS method was subsequently used to identify the most balanced solution.

Figure 7 presents the three-dimensional Pareto front generated by NSGA-II optimization. Each point represents a feasible composition that satisfies the predefined compositional constraints. The distribution of Pareto solutions demonstrates the inherent trade-off relationship among magnetic performance, cost, and the GWP indicator. Because no single candidate simultaneously provides the highest predicted magnetic performance and the lowest economic and environmental indicators, the Pareto set offers a range of alternative designs rather than a unique optimum.

The candidate with the highest TOPSIS score was selected as the final compromise solution, and its composition and objective values are summarized in Table 3. The selected candidate contains rare-earth sublattice fractions of approximately 0.79 Ce, 0.01 La, 0.01 Y, 0.01 Pr, and 0.18 Nd. With a total rare-earth

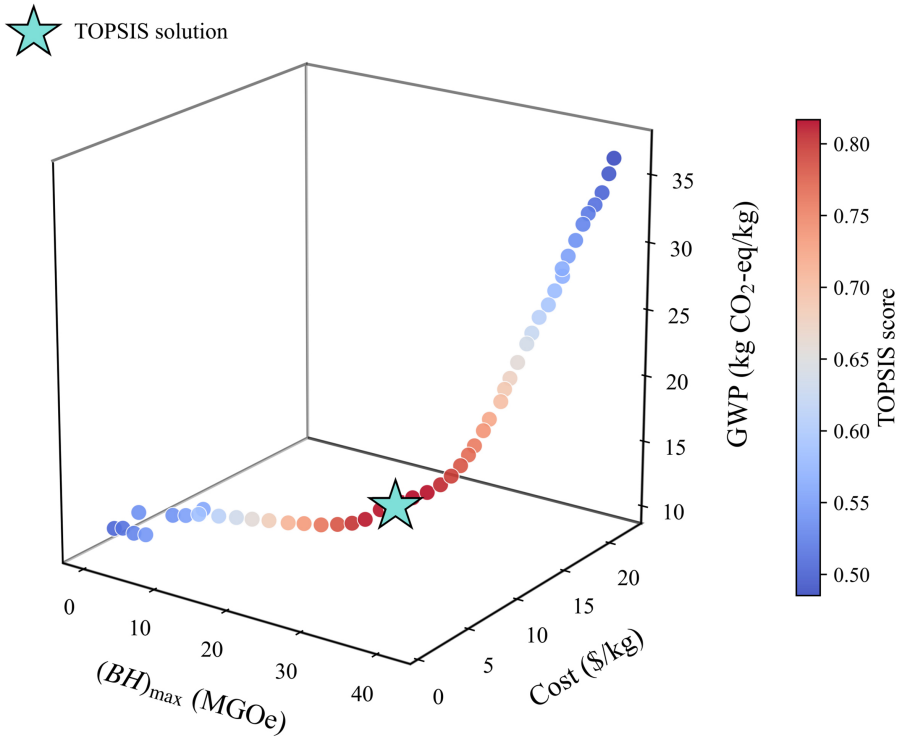

Figure 7. Pareto front obtained from NSGA-II multi-objective optimization. The color scale represents the TOPSIS score, and the marked point indicates the final selected compromise solution. NSGA-II: Non-dominated sorting genetic algorithm II; TOPSIS: Technique for Order Preference by Similarity to Ideal Solution; GWP: global warming potential.

Table 3. Composition variables and objective values of the TOPSIS-selected solution

	Variables	Values
Input variables	P_{Ce}	0.79
	P_{La}	0.01
	P_{Y}	0.01
	P_{Pr}	0.01
	P_{Nd}	0.18
	P_{REs}	24.19
	P_{Fe}	75.28
	P_{Co}	0.03
	P_{B}	0.50
	P_{TM}	< 0.01
Objective values	Price ($/kg)	4.78
	GWP (kg CO_2-eq/kg)	16.41
	$(BH)_{max}$ (MGOe)	35.16

TOPSIS: Technique for Order Preference by Similarity to Ideal Solution; GWP: global warming potential.

content of approximately 24.19 wt.%, these fractions correspond to approximately 19.11 wt.% Ce and 4.35 wt.% Nd in the overall magnet composition. The remaining major constituents are approximately 75.28 wt.% Fe, 0.03 wt.% Co, and 0.50 wt.% B, while the TM content is constrained below 0.01 wt.%.

The selected composition achieves a predicted $(BH)_{max}$ of 35.16 MGOe, together with an estimated material cost of 4.78 $/kg and a composition-related GWP value of 16.41 kg CO_2-eq/kg. Rather than representing the

individual optimum of any single objective, this candidate provides a balanced compromise among magnetic performance, economic cost, and upstream environmental burden. The high Ce fraction and reduced Nd content demonstrate the potential of the proposed framework for identifying Ce-rich compositions that reduce reliance on Nd-rich designs while retaining competitive predicted magnetic performance.

It should be emphasized that the optimized composition is a data-driven screening candidate rather than an experimentally validated magnet. The current surrogate model is primarily based on elemental composition descriptors and does not explicitly account for phase stability, phase fractions, grain-boundary structure, processing conditions, or manufacturing-stage environmental impacts. Therefore, thermodynamic assessment, micromagnetic analysis, synthesis, and experimental characterization are required before practical conclusions can be drawn.

CONCLUSIONS

This study developed an integrated data-driven framework for the sustainable design of high-abundance rare-earth permanent magnets by combining ML prediction, SHAP-based interpretation, and multi-objective optimization. Unlike conventional composition optimization approaches that mainly focus on maximizing magnetic performance, the proposed framework simultaneously considers magnetic properties, economic cost, and a composition-related GWP indicator, providing a systematic strategy for exploring performance-resource-environment trade-offs.

Eight regression algorithms were systematically compared using a dataset of 346 literature-derived experimental records. Among the investigated models, the optimized MLP model exhibited the most balanced predictive performance after hyperparameter optimization and architecture adjustment. The final model achieved high predictive accuracy, with independent test R^2 values of 0.979, 0.901, and 0.955 for Br, H_{cj}, and $(BH)_{max}$, respectively. Repeated five-fold cross-validation further supported the robustness of the model, demonstrating that the prediction capability was not solely dependent on a specific data partition.

SHAP analysis provided an interpretable understanding of the ML model by identifying the contribution of different elemental variables to magnetic property prediction. Nd was found to be the most influential feature, consistent with its critical role in high-performance rare-earth magnets. Meanwhile, high-abundance rare-earth elements such as Ce and La also showed significant statistical contributions, indicating complex nonlinear substitution-related patterns within the investigated composition space. These results provide valuable guidance for subsequent composition exploration while emphasizing that SHAP-derived relationships represent statistical associations rather than direct physical mechanisms.

Based on the optimized MLP surrogate model, a multi-objective optimization framework combining NSGA-II and TOPSIS was established to identify balanced magnet compositions. This framework identified a balanced Ce-rich candidate with a predicted $(BH)_{max}$ of 35.16 MGOe, an estimated material cost of 4.78 $/kg, and a composition-related GWP indicator of 16.41 kg CO_2-eq/kg. The rare-earth sublattice of the selected candidate contains approximately 79% Ce and 18% Nd, corresponding to approximately 19.11 wt.% Ce and 4.35 wt.% Nd in the overall magnet composition. These results suggest that the proposed framework can identify promising composition regions that reduce reliance on Nd-rich formulations while maintaining competitive predicted magnetic performance.

Despite the promising prediction and optimization results, the optimized composition should be regarded as a data-driven candidate rather than an experimentally validated material. The current model mainly relies on elemental composition descriptors and does not explicitly incorporate phase stability, microstructural characteristics, or processing parameters. Future studies integrating additional physical descriptors and

experimental validation will further improve the reliability and practical applicability of the proposed framework.

Overall, this work demonstrates that the combination of interpretable ML and multi-objective optimization can accelerate the discovery of sustainable rare-earth permanent magnets. The proposed methodology provides a potential framework for designing advanced functional materials under simultaneous performance, resource, and environmental constraints.

DECLARATIONS

Authors' contributions

Conception and design of the study and methodology: Wu, Y.; Wang, L.; Wang, Q.
Data analysis and interpretation: Wu, Y.; Zhao, S.; Li, Q.
Data visualization and manuscript drafting: Wu, Y.; Zhang, Q.
Project administration and coordination: Wang, L.; Wang, Q.
Resources and experimental support: Wang, L.; Yu, H.; Wu, D.; Wu, F.
Supervision and scientific guidance: Wang, L.; Yu, H.; Wu, D.; Wu, F.; Wang, Q.
Manuscript review, editing, and critical revision: Wu, Y.; Wang, L.; Yu, H.; Wu, D.; Wu, F.; Wang, Q.
All authors read and approved the final manuscript.

Availability of data and materials

The complete dataset used in this study was compiled from literature-reported experimental data and cannot be publicly released due to licensing and source restrictions. The model settings and analysis code are available from the corresponding author upon reasonable request.

AI and AI-assisted tools statement

Not applicable.

Financial support and sponsorship

This work was financially supported by the Key Research Base Project for Philosophy and Social Sciences of Jiangxi Province (No. 25ZXSKJD05), the National Natural Science Foundation of China (Grant Nos. 72542009 and 52270192), the Key Laboratory of Rare Earths, Chinese Academy of Sciences (Grant No. E456F003) and the Key Laboratory of Ionic Rare Earth Resources and Environment, Ministry of Natural Resources of the People's Republic of China (No. 2023IRERE301).

Conflicts of interest

All authors declared that there are no conflicts of interest.

Ethical approval and consent to participate

Not applicable.

Consent for publication

Not applicable.

Supplementary Materials

Supplementary Materials

REFERENCES

1. Su, P.; Diao, C.; Tang, Y.; Yan, C. Review on progress of rare earth molecule-based functional materials in 2025. *J. Rare. Earths.* **2026**, *44*, 2249-58. DOI

2. Prados, T. M.; Barroso, T. L. C. T.; Forster-Carneiro, T.; Lovón-Canchumani, G. A.; Colpini, L. M. S. Life cycle assessment and circular economy in the production of rare earth magnets: an updated and comprehensive review. *Clean. Technol. Environ. Policy.* **2025**, *27*, 471-94. DOI
3. Wang, Q.; Wang, L.; Zhao, S.; Li, F.; Chen, W.; Wang, P. A critical life cycle assessment of present and potential rare earth circularity routes from permanent magnets. *Resour. Conserv. Recycl.* **2025**, *215*, 108106. DOI
4. Fritz, A. G.; Tarka, T. J.; Mauter, M. S. Assessing the economic viability of unconventional rare earth element feedstocks. *Nat. Sustain.* **2023**, *6*, 1103-12. DOI
5. Pei, K.; Zhang, X.; Lin, M.; Yan, A. Effects of Ce-substitution on magnetic properties and microstructure of Nd–Pr–Fe–B melt-spun powders. *J. Magn. Magn. Mater.* **2016**, *398*, 96-100. DOI
6. Zhu, M.; Han, R.; Li, W.; et al. An enhanced coercivity for (CeNdPr)–Fe–B sintered magnet prepared by structure design. *IEEE. Trans. Magn.* **2015**, *51*, 1-4. DOI
7. Xi, L.; Li, A.; Feng, H.; Tan, M.; Zhu, M.; Li, W. Phase structure of Al doped Ce-rich alloys and its effect on magnetic properties of sintered Ce-Fe-B magnets. *J. Alloys. Compd.* **2019**, *782*, 723-8. DOI
8. Skoug, E. J.; Meyer, M.; Pinkerton, F.; Tessema, M. M.; Haddad, D.; Herbst, J. Crystal structure and magnetic properties of $Ce_2Fe_{14-x}Co_xB$ alloys. *J. Alloys. Compd.* **2013**, *574*, 552-5. DOI
9. Feng, Q.; Huang, D.; Zhao, L.; et al. Overcoming refractory $REFe_2$ phase bottleneck in high-Ce Nd–Ce–Fe–B magnets via praseodymium-induced phase transformation: enabling liquid-phase grain boundary diffusion of dysprosium. *Adv. Funct. Mater.* **2026**, *36*, e25964. DOI
10. Cheng, M.; Fu, C. L.; Okabe, R.; et al. Artificial intelligence-driven approaches for materials design and discovery. *Nat. Mater.* **2026**, *25*, 174-90. DOI PubMed
11. Qin, X.; Wang, Q.; Zhao, X.; et al. A property-oriented self-decision design strategy of low-alloyed rare earth-free magnesium alloys with a good strength-ductility synergy based on machine learning. *J. Mater. Inf.* **2025**, *5*, 13. DOI
12. Jordan, M. I.; Mitchell, T. M. Machine learning: trends, perspectives, and prospects. *Science* **2015**, *349*, 255-60. DOI PubMed
13. Cheng, W. Magnetic remanence prediction of NdFeB magnets based on a novel machine learning intelligence approach using a particle swarm optimization support vector regression. *Int. J. Softw. Sci. Comput. Intell.* **2014**, *6*, 72-81. DOI
14. Zhang, Y.; Xu, X. Predicting magnetic remanence of NdFeB magnets from composition. *J. Supercond. Nov. Magn.* **2021**, *34*, 2711-5. DOI
15. Qiao, Z.; Dong, S.; Li, Q.; et al. Performance prediction models for sintered NdFeB using machine learning methods and interpretable studies. *J. Alloys. Compd.* **2023**, *963*, 171250. DOI
16. Konak, A.; Coit, D. W.; Smith, A. E. Multi-objective optimization using genetic algorithms: a tutorial. *Reliab. Eng. Syst. Saf.* **2006**, *91*, 992-1007. DOI
17. Pereira, J. L. J.; Oliver, G. A.; Francisco, M. B.; Cunha, S. S.; Gomes, G. F. A review of multi-objective optimization: methods and algorithms in mechanical engineering problems. *Arch. Comput. Methods. Eng.* **2022**, *29*, 2285-308. DOI
18. Nuhanović, A.; Hivziefendić, J.; Hadžimehmedović, A. Distribution network reconfiguration considering power losses and outages costs using genetic algorithm. *J. Electr. Eng.* **2013**, *64*, 265-71. DOI
19. Dou, M.; Jia, R.; Li, G. An optimization model of sewage discharge in an urban wetland based on the multi-objective wolf pack algorithm. *Environ. Monit. Assess.* **2019**, *191*, 763. DOI
20. Wang, Z.; Zhang, X.; Zhang, Z.; Sheng, D. Credit portfolio optimization: a multi-objective genetic algorithm approach. *Borsa. Istanb. Rev.* **2022**, *22*, 69-76. DOI
21. Khatamsaz, D.; Vela, B.; Singh, P.; Johnson, D. D.; Allaire, D.; Arróyave, R. Multi-objective materials bayesian optimization with active learning of design constraints: design of ductile refractory multi-principal-element alloys. *Acta. Mater.* **2022**, *236*, 118133. DOI
22. Zhang, G.; Wang, Y.; Meng, X.; et al. Life cycle assessment on the vanadium production process: a multi-objective assessment under environmental and economic perspectives. *Resour. Conserv. Recycl.* **2023**, *192*, 106926. DOI
23. Zeraati, M.; Arshadizadeh, R.; Chauhan, N. P. S.; Sargazi, G. Genetic algorithm optimization of magnetic properties of Fe-Co-Ni nanostructure alloys prepared by the mechanical alloying by using multi-objective artificial neural networks for the core of transformer. *Mater. Today. Commun.* **2021**, *28*, 102653. DOI
24. Wakjira, T. G.; Kutty, A. A.; Alam, M. S. A novel framework for developing environmentally sustainable and cost-effective ultra-high-performance concrete (UHPC) using advanced machine learning and multi-objective optimization techniques. *Constr. Build. Mater.* **2024**, *416*, 135114. DOI
25. Pandey, D.; Niwaria, K.; Chourasia, B. Machine learning algorithms: a review. *Int. Res. J. Eng. Technol.* **2019**, *6*, 916-22. https://www.irjet.net/archives/V6/i2/IRJET-V6I2176.pdf. (accessed on 17 Aug 2026).
26. Nagelkerke, N. J. D. A note on a general definition of the coefficient of determination. *Biometrika* **1991**, *78*, 691-2. DOI

27. Hodson, T. O. Root mean square error (RMSE) or mean absolute error (MAE): when to use them or not. *Geosci. Model. Dev. Discuss.* **2022**, *15*, 5481-7. DOI
28. Belle, V.; Papantonis, I. Principles and practice of explainable machine learning. *Front. Big. Data.* **2021**, *4*, 688969. DOI PubMed PMC
29. Ikhlayel, M. Evaluation of the environmental impacts of rare earth elements production. *Int. J. Environ. Stud.* **2017**, *74*, 939-57. DOI
30. Lee, J. C.; Wen, Z. Rare earths from mines to metals: comparing environmental impacts from China's main production pathways. *J. Ind. Ecol.* **2017**, *21*, 1277-90. DOI
31. Schreiber, A.; Marx, J.; Zapp, P.; Kuckshinrichs, W. Comparative life cycle assessment of neodymium oxide electrolysis in molten salt. *Adv. Eng. Mater.* **2020**, *22*, 1901206. DOI
32. Ferreira, H.; Leite, M. G. P. A life cycle assessment study of iron ore mining. *J. Clean. Prod.* **2015**, *108*, 1081-91. DOI
33. Farjana, S. H.; Huda, N.; Mahmud, M. P. Life cycle assessment of cobalt extraction process. *J. Sustain. Min.* **2019**, *18*, 150-61. DOI
34. Liu, L. F.; Gao, F.; Wang, S. B.; Wang, Z. H.; Gong, X. Z.; Li, X. Q. Life cycle environmental impact assessment of amorphous alloy strips production. *Mater. Sci. Forum.* **2016**, *847*, 328-34. DOI
35. Deb, K.; Pratap, A.; Agarwal, S.; Meyarivan, T. A fast and elitist multiobjective genetic algorithm: NSGA-II. *IEEE. Trans. Evol. Computat.* **2002**, *6*, 182-97. DOI
36. Etghani, M. M.; Shojaeefard, M. H.; Khalkhali, A.; Akbari, M. A hybrid method of modified NSGA-II and TOPSIS to optimize performance and emissions of a diesel engine using biodiesel. *Appl. Therm. Eng.* **2013**, *59*, 309-15. DOI
37. Yoon, K. P.; Hwang, C. L. Multiple attribute decision making: an introduction. Sage Publications. Inc.: 1995. DOI
38. Chakraborty, S. TOPSIS and modified TOPSIS: a comparative analysis. *Decis. Anal. J.* **2022**, *2*, 100021. DOI
39. Hesthaven, J.; Ubbiali, S. Non-intrusive reduced order modeling of nonlinear problems using neural networks. *J. Comput. Phys.* **2018**, *363*, 55-78. DOI
40. Zhao, C.; Jiang, Q.; Rehman, S. U.; et al. Effect of La–Y co-substitution on magnetic properties and microstructure of NdFeB alloy ribbons. *J. Rare. Earths.* **2022**, *40*, 1894-8. DOI
41. Xu, K.; Li, H.; Luo, Y.; et al. Experimental and computational study on the phase formation and magnetic properties of Ce-La-Fe-B alloys. *J. Magn. Magn. Mater.* **2018**, *461*, 100-5. DOI